Blood Vessel Segmentation in Retinal Images based on Local Binary Patterns and Evolutionary Neural Networks

Antonio Rodríguez-Jiménez and Enrique J. Carmona

Dpto. de Inteligencia Artificial, ETSI Informática, Universidad Nacional de Educación a Distancia (UNED), Juan del Rosal 16, 28040, Madrid, Spain
arodri@ea.mde.es
ecarmona@dia.uned.es

Abstract. This paper presents a method for the segmentation of the blood vessels, which form the retinal vascular network, in color fundus photographs. It is based on the idea of local binary pattern operators (LBP, LTP, CLBP) and evolutionary neural networks. Thus, a new operator, called SMLBP, is used to obtain a feature vector for every pixel in the image. Then we build a data set out of these features and train an evolutionary artificial neural network (ANN). We do not use a classical method for training ANN. Instead, we use an evolutionary algorithm based on grammatical evolution. The evaluation of the method was carried out using two of most used digital retinal image databases in this field: DRIVE and STARE. The method obtains competitive performance over other methods available in the relevant literature in terms of accuracy, sensitivity and specificity. One of the strengths of our method is its low computational cost, due to its simplicity.

Keywords: Blood vessel segmentation, retinal images, local binary patterns, evolutionary artificial neural networks, grammatical evolution.

1 Introduction

The study of the retinal blood vessel network provides useful information to ophthalmologists for the diagnosis of many ocular diseases. Thus, certain pathologies, such as diabetic retinopathy, hypertension, atherosclerosis or macular degeneration age, can affect the vessels morphology causing changes in their diameter, tortuosity or branching angle. The manual retinal vascular network segmentation requires much training and skill, and is therefore a slow process. Consequently, the appearance of automatic segmentation methods implies a great advantage for both the diagnosis and monitoring of retinal diseases, provided they are fast and efficient. Over the last few decades, different methods for segmenting the vascular network have been emerging. Basically, in the relevant literature, we found two ways of approaching the problem: either through unsupervised methods [1,2,3,4,17,18] or by supervised methods [5,8,11,12,13,14]. The method presented in this paper belongs to the second group. Basically, it is based on the extraction of LBP features from the retinal images and these will be used to train an evolutionary artificial neural network (EANN). Once the EANN is built, each pixel of a new image can be labeled as belonging or not to blood vessels.

The article is organized as follows. Section 2 describes the proposed segmentation method. In section 3, we test the performance of our method and compare with other competitive segmentation methods. Finally, section 4 presents the conclusions.

2 Description of the Segmentation Method

Building the feature vector

Local Binary Patterns (LBP) [9] are a type of features very frequently used for textures classification in computer vision. An important property of LBP is its invariance to rotation and illumination changes. The calculation of that feature consists of comparing the intensity of a pixel, g_c, with its neighboring P pixels, g_p, uniformly spaced on a radius R, and considering the result of each comparison as a bit in a binary string. In that comparison, only the sign, $s(x)$, is considered:

$$LBP_{P,R} = \sum_{p=0}^{P-1} s(g_p - g_c)2^p, \quad \text{where } s(x) = \begin{cases} 1, & x \geq 0 \\ 0, & x < 0 \end{cases} \tag{1}$$

The result of (1) is a single number characterizing the local texture of the image. This operator is monotonic grayscale transformation invariant. To make it rotation invariant ("ri"), Ojala et al. [9] defined the $LBP^{ri}_{P,R}$ operator:

$$LBP^{ri}_{P,R} = min\{ROR(LBP_{P,R}, i) \mid i = 0, 1, \ldots, P-1\} \tag{2}$$

where $ROR(x, i)$ performs a circular bit-wise right shift on the P-bit number, x, i-times.

Since we are trying to detect geometric patterns instead of textures, we experimented with several variations of the LBP operator, such as LTP [15] and $CLBP$ [19]. Finally, we introduce in this paper a new operator, called *sign-magnitude LBP* (SMLBP), which has six rotation invariant components, $S^{ri}_{P,R}$, $PS^{ri}_{P,R}$, $NS^{ri}_{P,R}$, $M^{ri}_{P,R}$, $PM^{ri}_{P,R}$ and $NM^{ri}_{P,R}$. The first three are related to sign (S) values, positive (PS) and negative (NS), and the last three to magnitude (M) values, positive (PM) and negative (NM). Thus, $SMLBP\_S^{ri}_{P,R}$ is the same as $LBP^{ri}_{P,R}$ (see eq. (2)). The values of $SMLBP\_PS^{ri}_{P,R}$ and $SMLBP\_NS^{ri}_{P,R}$ are evaluated as the rotation invariant versions of the positive (LTP_PS) and negative (LTP_NS) components of LTP:

$$SMLBP\_PS^{ri}_{P,R} = min\{ROR(LTP\_PS_{P,R}, i) \mid i = 0, 1, \ldots, P-1\} \tag{3}$$

$$SMLBP\_NS^{ri}_{P,R} = min\{ROR(LTP\_NS_{P,R}, i) \mid i = 0, 1, \ldots, P-1\} \tag{4}$$

where

$$LTP\_PS_{P,R} = \sum_{p=0}^{P-1} s(g_p - (g_c + \delta))2^p, \quad \text{and } s(x) = \begin{cases} 1, & g_p \geq g_c + \delta \\ 0, & \text{otherwise} \end{cases} \tag{5}$$

$$LTP\_NS_{P,R} = \sum_{p=0}^{P-1} s(g_p - (g_c - \delta))2^p, \quad \text{and } s(x) = \begin{cases} 1, & g_p \leq g_c - \delta \\ 0, & \text{otherwise} \end{cases} \tag{6}$$

and $\delta > 0$ is a threshold selected by the user. The first component, concerning magnitude, $SMLBP\_M^{ri}_{P,R}$, is equivalent to the rotation invariant version of component $CLBP\_M$ in $CLBP$:

$$SMLBP\_M^{ri}_{P,R} = min\{ROR(CLBP\_M_{P,R}, i) \mid i = 0, 1, \ldots, P-1\} \tag{7}$$

where

$$CLBP\_M_{P,R} = \sum_{p=0}^{P-1} t(m_p, c)2^p, \quad \text{and } t(x,c) = \begin{cases} 1, & x \geq c \\ 0, & x < c \end{cases} \tag{8}$$

and where $m_p = |g_p - g_c|$, and c is calculated as the average value of $|g_p - g_c|$, for all pixels of the image. Finally, based on the mixture of LTP and $CLBP\_M$, we give the following definitions to build the last two components, $SMLBP\_PM^{ri}_{P,R}$ and $SMLBP\_NM^{ri}_{P,R}$:

$$SMLBP\_PM^{ri}_{P,R} = min\{ROR(SMLBP\_PM_{P,R}, i) \mid i = 0, 1, \ldots, P-1\} \tag{9}$$

$$SMLBP\_NM^{ri}_{P,R} = min\{ROR(SMLBP\_NM_{P,R}, i) \mid i = 0, 1, \ldots, P-1\} \tag{10}$$

where

$$SMLBP\_PM_{P.R} = \sum_{p=0}^{P-1} t(m_p, c)2^p, \quad \text{and } t(x,c) = \begin{cases} 1, & x \geq c + \delta \\ 0, & \text{otherwise} \end{cases} \tag{11}$$

$$SMLBP\_NM_{P.R} = \sum_{p=0}^{P-1} t(m_p, c)2^p, \quad \text{and } t(x,c) = \begin{cases} 1, & x \leq c - \delta \\ 0, & \text{otherwise} \end{cases} \tag{12}$$

and where m_p, c and δ have the same meaning as the above equations.

Building the evolutionary neural network

In order to train the ANN, a training dataset is build from the training DRIVE image database [14], which is composed of 20 images. For each training RGB image, the following steps are applied: (i) we select the green channel because it is assumed that this channel gives the highest contrast between vessel and background [4]; (ii) a Gaussian filtering is used in that channel to remove noise, mainly due to the digitization of the image; (iii) the operators $SMLBP^{ri}_{P,R}$, with $R = \{r_1, \ldots, r_m\}$ and $P = \{p_1, \ldots, p_n\}$, is applied to the image pixels. Thus, each register of the training dataset is composed of a feature vector of $6 \times m \times n$ components, plus an additional component that stores the class value (*vessel* o *non-vessel*). For each training image, the vessel features are obtained from all the vessel pixels, according to the gold standard mask. On the other hand, non-vessel features are obtained randomly from the rest of non-vessel pixels, by sampling an amount of non-vessel pixels equal to the number of vessel pixels.

We use an evolutionary algorithm to build the ANN. It was implemented using grammatical evolution [10] and is based on the grammar proposed in [16]. The final ANN obtained is a classical multilayer perceptron (MLP) that is obtained by selecting the best MLP of a population of MLPs. This population corresponds to the final evolved population that results of running the evolutionary algorithm. This kind of algorithms allows designing the topology of the network without user's intervention. Thus they adjust automatically the connection weights, select automatically the number of neurons in the hidden layer and also select automatically, from the initial set of feature inputs, the most discriminant features as inputs. The net obtained, called *ANN of vessels* (ANN_V), was trained with $SMLBP^{ri}_{P,R}$ vector, selecting $R = \{1, 2, \ldots, 9\}$ and $P = \{24\}$.

In order to further improve the accuracy of previous ANN, a new net, called *ANN of thin vessels* (ANN_TV), is build. As its name indicates, that net is specialized in detecting thin blood vessels. The ANN_TV building procedure is the same as that one used with ANN_V. Previously, an image dataset of thin vessel was build. Thus, for each vessel mask from the training DRIVE mask database, we apply a tophat transformation, with disk shaped structuring element of radius equal to one pixel. The result is a set of training masks with only thin vessels. Finally, the ANN_TV was trained with $SMLBP^{ri}_{P,R}$ vectors, selecting $R = \{1, 2, 3\}$ and $P = \{24\}$.

Segmentation method

Fig. 1 shows a block diagram of the segmentation process, once the two ANNs have been trained. An example of the output of each block can be also seen in fig. 2, as result of processing a input RGB retinal image. Thus, first of all, a Gaussian filter is applied to the green channel of the input RGB image (fig. 2a). Then the output of ANN_TV (fig. 2b) and ANN_V (fig. 2c) are calculated, using the filtered green channel as input. Afterward the ANN_TV output is thresholded and binarized (fig. 2d). A threshold is also applied to the ANN_V output for assigning zeros to all the pixels below to that threshold (fig. 2e). Subsequently, for adding the information provided from red and blue channels of the image, these two channel and the output produced by the ANN_V are normalized and used as inputs to a k-means algorithm, with $k = 2$. Two cluster are obtained: one of them is associated to noise, usually belonging to the bright part of the papilla, and the other corresponds to a binary image of blood vessels (fig. 2f). Then a logical OR operator is applied, using as inputs the binarized output of ANN_TV and the binarized vessel cluster, to obtain a first approximation to the binary segmentation mask of retinal vascular network (fig. 2g). However, this segmentation has a lot of noise in the form of little blobs. Finally, these blobs are removed with a blob size filter (fig. 2h).

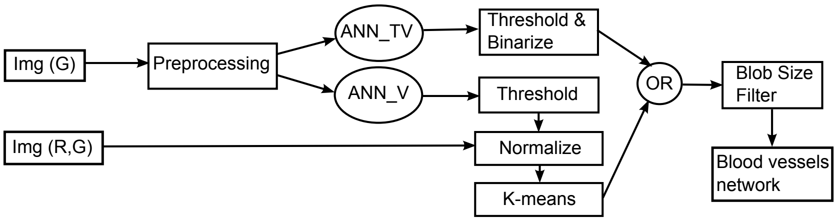

Fig. 1: Block diagram of the segmentation process.

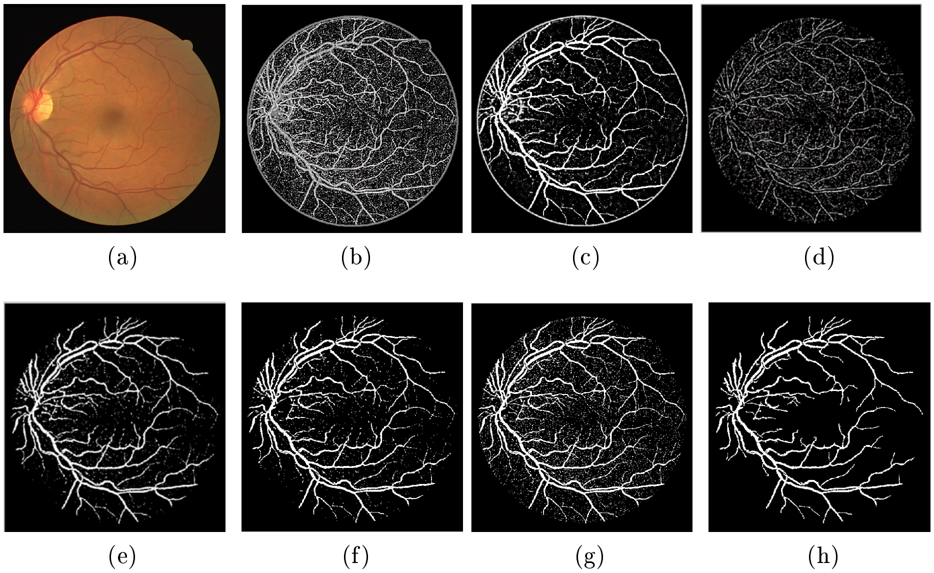

Fig. 2: Output resulting from each stage of the segmentation process described in Fig. 1: (a) Original image, (b) ANN_TV, (c) ANN_V, (d) thresholded ANN_TV, (e) thresholded ANN_V, (f) K-Means cluster, (g) OR operator, (h) Blob size filtering.

3 Results and Discussion

The ANN_V obtained from the training phase is composed of two neurons in the hidden layer and only four inputs ($PM_{5,24}^{ri}$, $NM_{5,24}^{ri}$, $M_{8,24}^{ri}$, $PS_{9,24}^{ri}$) of the fifty-four available features. On the other hand, the ANN_TV obtained is composed of two neurons in the hidden layer and two inputs ($PS_{2,24}^{ri}$, $PM_{3,24}^{ri}$) of the eighteen available features. The best result of the segmentation method, in terms of mean accuracy, is obtained with an blob filter size of $\eta = 30$ pixels. However, it should be noted that, while the accuracy and specificity increase with η, the sensitivity has the opposite behavior. This effect is shown in Fig. 3

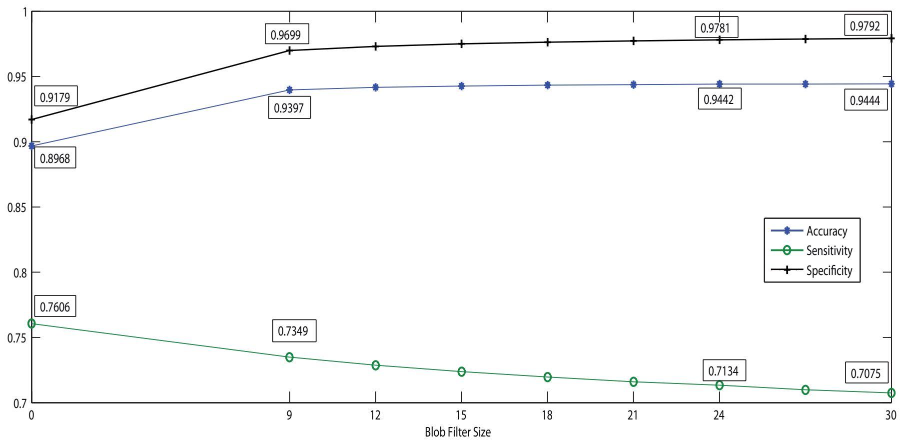

Fig. 3: Variation of accuracy, sensitivity and specificity (y-axis), as a function of the blob filter size,η, (x-axis), for the test DRIVE database.

Table 1, shows the accuracy, sensitivity and specificity of our method applied to the test images from DRIVE database ($\eta = 24$ and $\eta = 30$). These results are compared with those obtained by other vessels segmentation methods existing in the relevant literature. As it can be seen, our results are competitive.

To check the robustness of our segmentation method, we applied it in the STARE database [4]. The method was applied without changes, that is, we used the same ANNs as those trained from the DRIVE database. As it is shown in Table 2, despite the difference in the quality of the two image databases (worst in STARE), our segmentation results remain competitive.

Finally, Table 3 shows the computational cost of our method, compared to the other methods. From all the segmentation times reported in the literature (this information is not always available), our method is the fastest. The explanation for this behavior is based on the fact that our method only needs to compute six $SMLBP^{ri}$ features per pixel and the computational cost of evaluating the two ANNs is low.

Table 1: Performance of vessel segmentation methods (test DRIVE database)

Segmentation Method	Average Accuracy±SD	Sensitivity	Specificity
Lam et al[5]	0.9595	N.A	N.A
Ricci&Perfetti[11]	0.9595	N.A	N.A
2nd Human observer	0.9470±0.0048	0.7763	0.9725
Soares et al. [13]	0.9466±0.0058	0.7285	0.9786
Miri&Mahloojifar[7]	0.9458	0.7352	0.9795
Mendoça&Campilho[6]	0.9452±0.0062	0.7344	0.9764
Proposed Method ($\eta = 30$)(LBP+EANN)	0.9444±0.0065	0.7075	0.9768
Proposed Method ($\eta = 24$)(LBP+EANN)	0.9442±0.0065	0.7134	0.9781
Staal et al. [14]	0.9441±0.0065	0.6780	N.A
Fraz et al. [2]	0.9430±0.0072	0.7152	0.9768
Niemeijer et al. [8]	0.9416±0.0065	0.6898	0.9696
Zana&Klein [18]	0.9377±0.0077	0.6453	0.9769
Fraz et al.[3]	0.9303±0.0079	0.7114	0.9680

Table 2: Performance of vessel segmentation methods (STARE database)

Segmentation Method	Average Accuracy	Sensitivity	Specificity
Ricci and Perfetti [11]	0.9646	N.A	N.A
Lam et al. [5]	0.9567	N.A	N.A
Staal et al. [14]	0.9516	0.6970	0.9810
Soares et al. [13]	0.9478	0.7197	0.9747
Fraz et al. [2]	0.9442	0.7311	0.9680
Proposed Method($\eta = 30$) (LBP+EANN)	0.9371	0.7432	0.9592
Fraz et al. [3]	0.9367	0.6849	0.9710
2nd human observer	0.9348	0.8951	0.9384
Hoover et al. [4]	0.9275	0.7500	0.9562

Table 3: Running times (per image) for different vessel segmentation methods

Method	Time	PC	Software
Proposed Method (LBP+EANN)	2.5 s	i5 3.1GHz, 8GB RAM	Matlab
Fraz (Bit plane slicing)[3]	35 s	Centrino, 2GHz, 1GB RAM	Matlab
Mendoça&Campilho[6]	2.5-3 m	Pentium 4, 3.2 GHz, 960 Mb RAM	Matlab
Soares et al. [13]	3 m	AMD Athlon XP2700, 2GHz, 1GB RAM	Matlab
Lam et al. [5]	13 m	Duo CPU 1.83 GHz, 2GB RAM	Matlab
Staal et al. [14]	15 m	Pentium III, 1.0 GHz, 1 GB RAM	Matlab

4 Conclusions

The segmentation method of blood vessels in retinal images, presented in this paper, obtains values of accuracy, sensitivity and specificity competitive with the best existing methods in the relevant literature concerning this matter. Moreover, from all the segmentation times reported, our method obtains the best segmentation time, because it only needs to calculate LBP values, whose cost is very low, and apply them to two ANNs which are already trained. It is also shown the advantage of using grammatical evolution for learning ANNs, avoiding the user's effort of designing the network topology (number of neurons in the hidden layer) and selecting the most discriminative input features. These two advantages allow obtaining ANNs fairly simple, compact and with great power of generalization, as evidenced by the competitive segmentation results obtained by applying our method to a database that is different from that used for training. This work also provides evidence of the utility of using LBP operators in detecting geometric patterns, in addition to their well-known properties in detecting textures.

Acknowledgment

This work was supported in part by funds of the Advanced Artificial Intelligence Master Program of the Universidad Nacional de Educación a Distancia (UNED), Madrid, Spain.

References

1. S. Chaudhuri, S. Chatterjee, N. Katz, M. Nelson, and M. Goldbaum. Detection of blood vessels in retinal images using two-dimensional matched filters. *IEEE Transactions on Medical Imaging*, 8(3):263–269, 1989.
2. M.M. Fraz, S.A. Barman, P. Remagnino, A. Hoppe, A. Basit, B. Uyyanonvara, A.R. Rudnicka, and C.G Owen. An approach to localize the retinal blood vessels using bit planes and centerline detection. *Computer Methods and Programs in Biomedicine*, 108(2):600 – 616, 2012.
3. M.M. Fraz, M. Y. Javed, and A. Basit. Evaluation of retinal vessel segmentation methodologies based on combination of vessel centerlines and morphological processing. In *Emerging Technologies, 2008. ICET 2008. 4th International Conference on*, pages 232–236, 2008.
4. A. Hoover, V. Kouznetsova, and M. Goldbaum. Locating blood vessels in retinal images by piecewise threshold probing of a matched filter response. *Medical Imaging, IEEE Transactions on*, 19(3):203–210, 2000.
5. B.S.Y. Lam, G. Yongsheng, and A.W-C. Liew. General retinal vessel segmentation using regularization-based multiconcavity modeling. *Medical Imaging, IEEE Transactions on*, 29(7):1369–1381, 2010.
6. A.M. Mendonça and A. Campilho. Segmentation of retinal blood vessels by combining the detection of centerlines and morphological reconstruction. *Medical Imaging, IEEE Transactions on*, 25(9):1200–1213, 2006.

7. M.S. Miri and A. Mahloojifar. Retinal image analysis using curvelet transform and multistructure elements morphology by reconstruction. *IEEE Transactions on Biomedical Engineering*, 58(5):1183–1192, 2011.
8. M. Niemeijer, J. Staal, B.. Ginneken, M. Loog, and M.D. Abramoff. Comparative study of retinal vessel segmentation methods on a new publicly available database. In *Medical Imaging 2004: Image Processing*, volume 5370, pages 648–656, 2004.
9. T. Ojala, M. Pietikäinen, and T. Mäenpää. Gray scale and rotation invariant texture classification with local binary patterns. In: Computer Vision, ECCV 2000 Proceedings, Lecture Notes in Computer Science 1842, Springer, 404-420, 2000.
10. M. O'Neill and C. Ryan. Grammatical evolution. *Evolutionary Computation, IEEE Transactions on*, 5(4):349–358, 2001.
11. E. Ricci and R. Perfetti. Retinal blood vessel segmentation using line operators and support vector classification. *IEEE Transactions on Medical Imaging*, 26(10):1357–1365, 2007.
12. C. Sinthanayothin, J.F. Boyce, H.L. Cook, and T.H. Willianson. Automated localization of the optic disc, fovea, and retinal blood vessels from digital colour fundus images. *British Journal of Ophthalmology*, 83(8):902–910, 1999.
13. J.V. Soares, J.J. Leandro, R.M. Cesar Jr, H.F. Jelinek, and M.J. Cree. Retinal vessel segmentation using the 2-d gabor wavelet and supervised classification. *IEEE Transactions on Medical Imaging*, 25(9):1214–1222, 2006.
14. J. Staal, M.D. Abramoff, M. Niemeijer, M.A. Viergever, and B. van Ginneken. Ridge-based vessel segmentation in color images of the retina. *Medical Imaging, IEEE Transactions on*, 23(4):501–509, 2004.
15. X. Tan and B. Triggs. Enhanced local texture feature sets for face recognition under difficult lighting conditions. *Image Processing, IEEE Transactions on*, 19(6):1635–1650, 2010.
16. I.G. Tsoulos, D. Gavrilis, and E. Glavas. Neural network construction using grammatical evolution. In *Signal Processing and Information Technology, 2005. Proceedings of the Fifth IEEE International Symposium on*, pages 827–831, 2005.
17. W. G. Xiaohong, A. Bharath, A. Stanton, A. Hughes, N. Chapman, and S. Thom. Quantification and characterisation of arteries in retinal images. *Computer Methods and Programs in Biomedicine*, 63(2):133 – 146, 2000.
18. F. Zana and J.C. Klein. Segmentation of vessel-like patterns using mathematical morphology and curvature evaluation. *Image Processing, IEEE Transactions on*, 10(7):1010–1019, 2001.
19. G. Zhenhua, D. Zhang, and D. Zhang. A completed modeling of local binary pattern operator for texture classification. *Image Processing, IEEE Transactions on*, 19(6):1657–1663, 2010.